CHAPTER- IX

MAXIMUM SHEAR MODULUS OF HOMOGENEOUS AND STRATIFIED SOIL-ASH DEPOSIT AND CORRELATION STUDIES

9.1 INTRODUCTION

The frequent occurrence of seismic activities now a days creates multiple issues in the Civil engineering structures, hence while designing these structures need special consideration of seismic loads. Seismic waves are normally propagated through the soil medium known as elastic body waves (P and S wave) and surface waves (Rayleigh and love wave). The ground shakings during seismic activities are governed by the shear wave velocity, i.e., higher velocity of shear wave attributes to less ground movement. It is dependent on the type of soil through which the wave passes such as, soft earth has a higher velocity than hard soil or rock (Khan 2013). The velocity of P and S waves are very significant parameter that is used to evaluate the constrained modulus and shear modulus respectively after simplifying the governing equations (Patel et al. 2012). The ratio of these body waves was also incorporated for the determination of Poisson's ratio of soil, that has been investigated by many researchers (Sawangsuriya et al. 2008; Fleureau et al. 2001; Sas et al. 2013; Patel et al. 2018). The main advantage of these dynamic parameters is that, it can be performed both in the field as well as in the laboratory. In addition, these can be estimated through non-destructive experiments that means repetition would be possible in the same specimen.

However, experiencing the current scenario of seismic activities the static evaluation would not be sufficient for the safe design of structures. Therefore, it is essential to investigate its behaviour or ground response analysis under dynamic excitation, for that along with dynamic properties, the normalized shear modulus is also needed. Hence, in this chapter the maximum shear modulus has been investigated for the homogeneous and stratified soil-ash deposit under various experimental conditions. The shear modulus deduced from the cyclic triaxial test has been incorporated with the maximum shear modulus to determine the normalized shear modulus of the present considered materials.

9.2 METHODOLOGY

The bender element works on the principle of piezoelectricity. Piezoelectricity is a phenomenon in which electric voltage applied to a piezoelectric element gets converted into mechanical vibration and vice versa. According to the wiring configuration (series and parallel), the piezo-ceramic can produce P and S waves. The detailed explanation regarding the working principle, wave types, and the factors affecting movement of the wave has been discussed by Ingale et al. (2017). The S wave generated through this element named as bender element. Whereas the P wave generated through this element named as extender element. The element is consisting of two ceramic plates that are separated by thin metallic plate. This test contains transmitter and receiver element, which is penetrated into the bottom and top of the soil specimen. Usually, transmitter situated at the bottom, which is subjected to electric voltage, that creates a bending of the element results in generation of S waves (Fig. 9.1). These generated S waves disturb the receiver element results in the conversion of electric voltage. The sinusoidal input wave has been subjected to soil through waveform generator and their respective response has been displayed on the oscilloscope. The travel time required for the input

wave from the transmitter to the receiver end has been investigated. The complete arrangements required for this bender element analysis have been shown in Fig. 9.2.

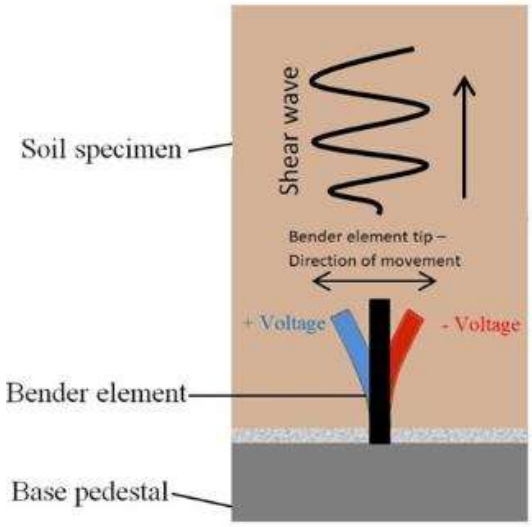

Fig. 9.1. Bender element vibration mechanism (Source: VJ tech).

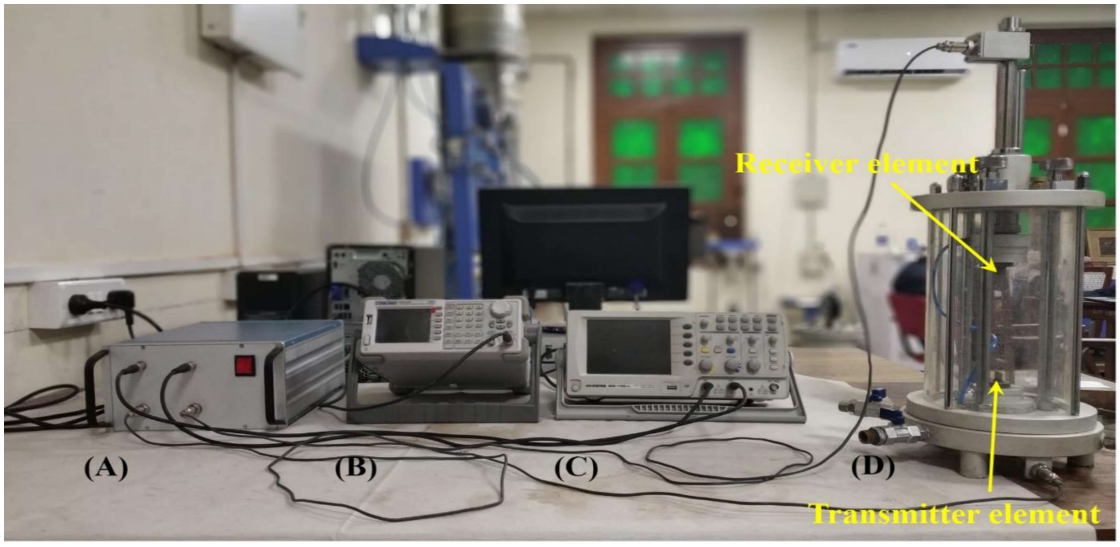

Fig. 9.2. Bender element complete setup, (a) amplifier, (b) waveform generator, (c) oscilloscope, and (d) triaxial setup equipped with bender element.

9.3 RESULTS AND DISCUSSION

In the present study, the bender element analysis has been performed considering both the homogeneous and stratified soil-ash arrangements. The samples were investigated for the specimen subjected to the confining pressure stage, saturated with confinement

stage, and saturated without confinement stage. The outcomes of the present experimental analysis have been briefly discussed in the subsequent sections.

9.3.1 Identification of an Appropriate Method for the Estimation of Shear Wave Velocity

The time required for the generated S wave to travel from the transmitter end to the receiver end is the main point of concern in the bender element test. This time difference is generally evaluated from the plot of input and output wave by implementing time domain and frequency domain approaches, and cross-correlation. These approaches were developed due to the involvement of several complexities such as the near field effect, cross talk effect, and wave attenuation (Sanchez-Salinero et al. 1986; Lee and Santamarina 2005; Wang et al. 2007; Patel et al. 2010). Also, it is highly recommended to implement tip to tip distance of the specimen for the velocity estimation through travel time. There is no standard available that can recommend the particular time determination method for a specific type of soil. Therefore, depending on the convenience of identification of travel time, time domain analysis has been subdivided into start-to-start, peak-to-peak, and trough-to-trough. The time domain analysis has a higher influence of the near field effect specially under low input frequency. The start-to-start approach is still disputed due to the presence of the near field effect, which poses a barrier to acquiring a clearer waveform. Viggiani and Atkinson (1995) implemented start-to-start approach in their investigation whereas Sanchez-Salinero et al. (1986) recommended to maintain suitable range of tip to tip length upon the wavelength of input wave in order to eliminate the near field effect. Similarly, the frequency domain approach works on the assumption that the frequency of the input wave must be same as that of the frequency of the output wave. In the same way, the

cross-correlation approach is considered in time domain approach, but its calculations were executed in the frequency domain approach.

The travel time difference estimated by the frequency domain method shows a significant variation with that obtained by the time domain method. Hence, time domain analysis is preferred to determine the time delay and the same has been incorporated in the present study. The velocity of shear wave evaluated from the three different time domain approaches in the case of homogeneous and stratified soil system has been shown in Fig. 9.3, 9.4, & 9.5. The implemented time domain approaches are start-to-start, peak-to-peak, and trough-to-trough. The start-to-start is a popular method, but this is largely influenced by the external factors. However, peak-to-peak is easy to perform and also recommended by various researchers (Arulnathan et al. 1998; Greening and Nash 2003). Hence, peak-to-peak method has been considered for the determination of the maximum shear modulus of the homogeneous and stratified soil-ash deposit in the present study.

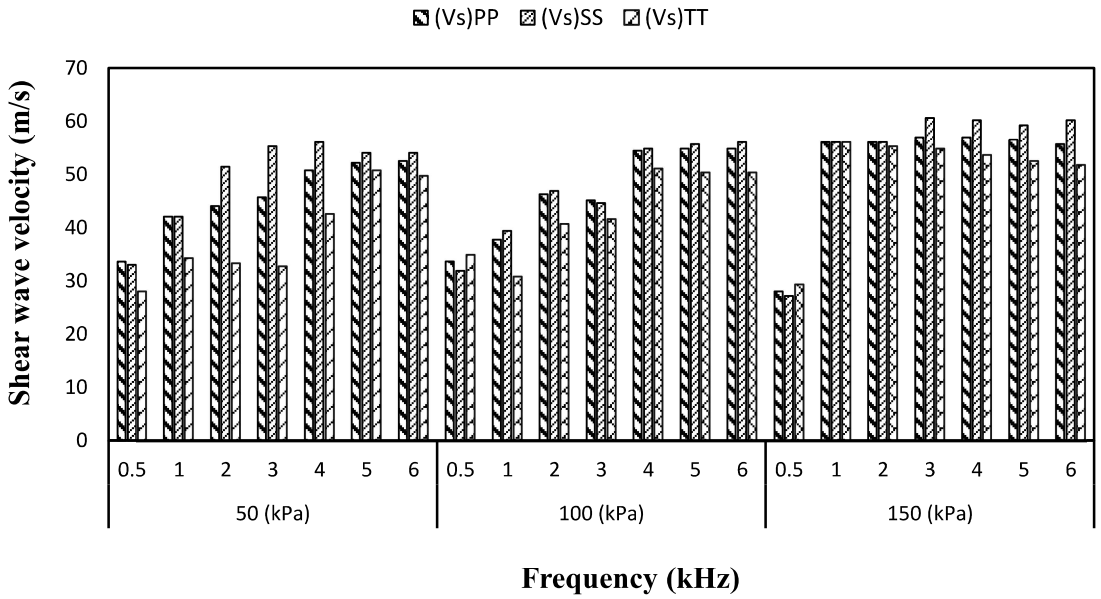

Fig. 9.3. Variation of shear wave velocity of fly ash determined through various available methods such as Peak to Peak, Start to Start, and Trough to Trough. (MDD:- 99%)

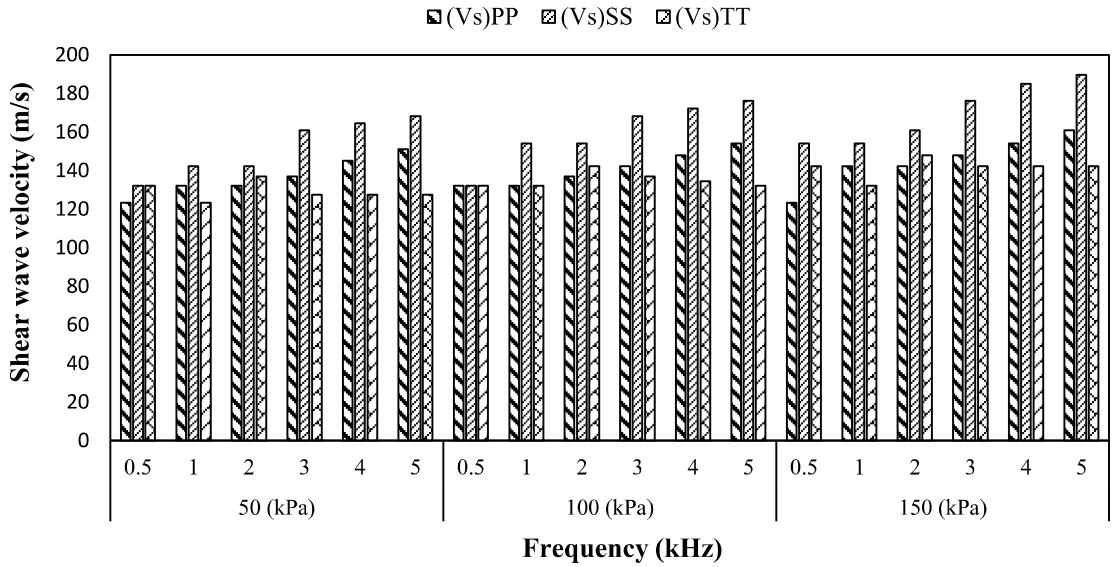

Fig. 9.4. Variation of shear wave velocity of local soil determined through various available methods such as Peak to Peak, Start to Start, and Trough to Trough. (MDD :- 99%)

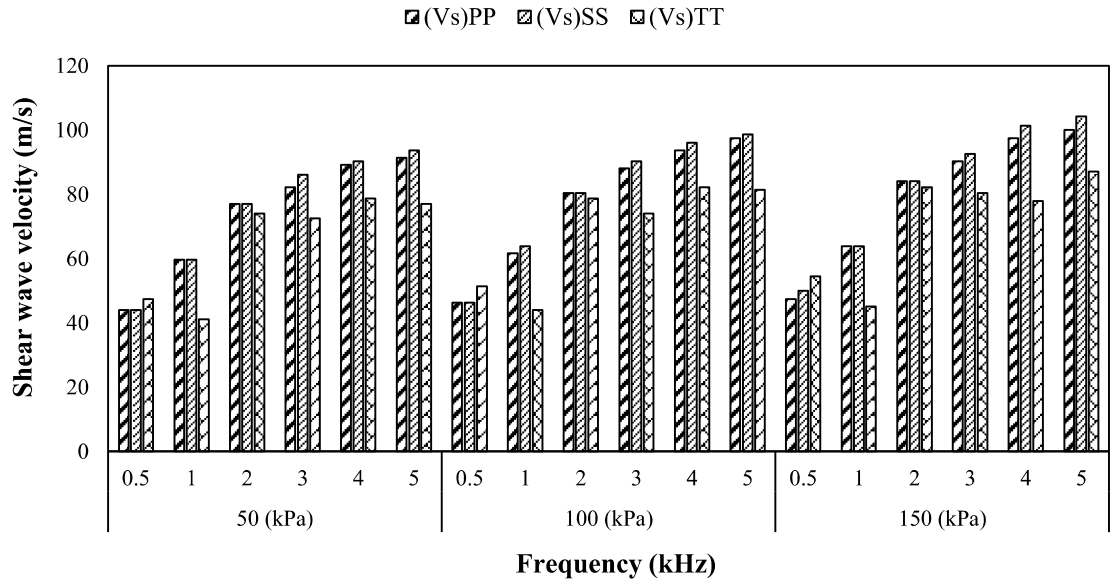

Fig. 9.5. Variation of shear wave velocity of Layered soil determined through various available methods such as Peak to Peak, Start to Start, and Trough to Trough. (MDD :- 95%)

9.3.2 Assessment of Maximum Shear Modulus of Homogeneous and Stratified Soil-Ash Deposit

The cylindrical specimen having 100 mm diameter and 50 mm height was used for the bender element test. The bender element of size 12 mm height and 12 mm width were inserted by making a groove at the center of the top and bottom of the specimen. The maximum shear modulus (G_{max}) estimated from the bender element test for both the homogeneous and stratified soil-ash system are presented in Fig. 9.6, 9.7, & 9.8. The experiments were conducted considering the specimen without lateral confinement, with confinement, and with saturation. These all conditions were taken to simulate the field conditions and also to assess the variation of G_{max} under these conditions. The outcome of this study (Fig. 9.6(b), 9.7(b), & 9.8(b)) shows that with the increase in the lateral confinement, G_{max} is also increasing significantly. This is due to the fact that higher confinement will exert high pressure on the surface area of the specimen that is attributed to the reduction in the size of the void. This reduced void creates less obstruction for the movement of the generated waves lead to the earlier detection, which increases the wave velocity that ultimately enhances the G_{max}. In the same way, all the figures exhibit incremental trend of G_{max} with the increase in the frequency of the input wave. However, the rate of increase in G_{max} was prominent upto the frequency of 3-4 kHz, after that this rate decreases. The G_{max} of the without confinement conditions experience minimum results followed by saturated condition and confinement. Also, the sample prepared under high relative compaction (RC) depicts high G_{max} except fly ash that happens due to the low-density variation under higher RC.

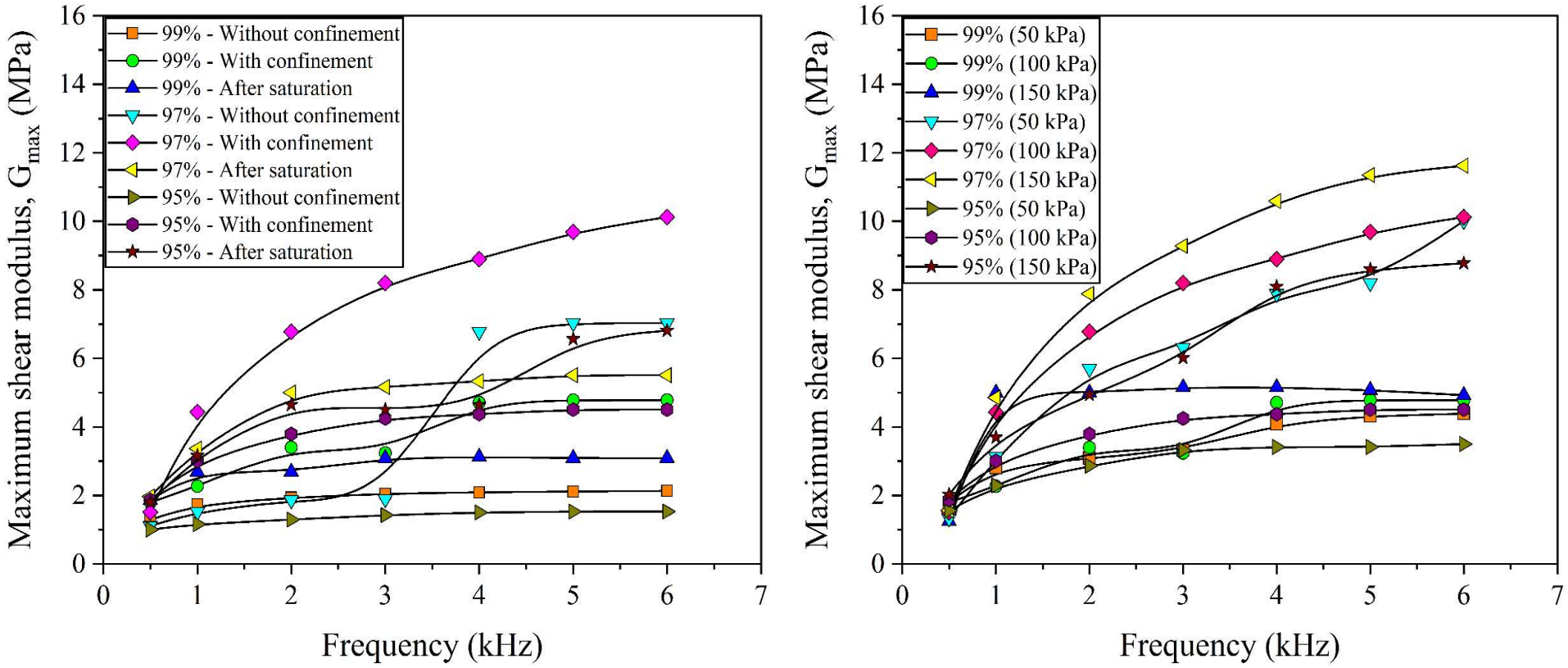

Fig. 9.6. Maximum shear modulus illustration of fly ash considering (a) all conditions and (b) under confinement without saturation.

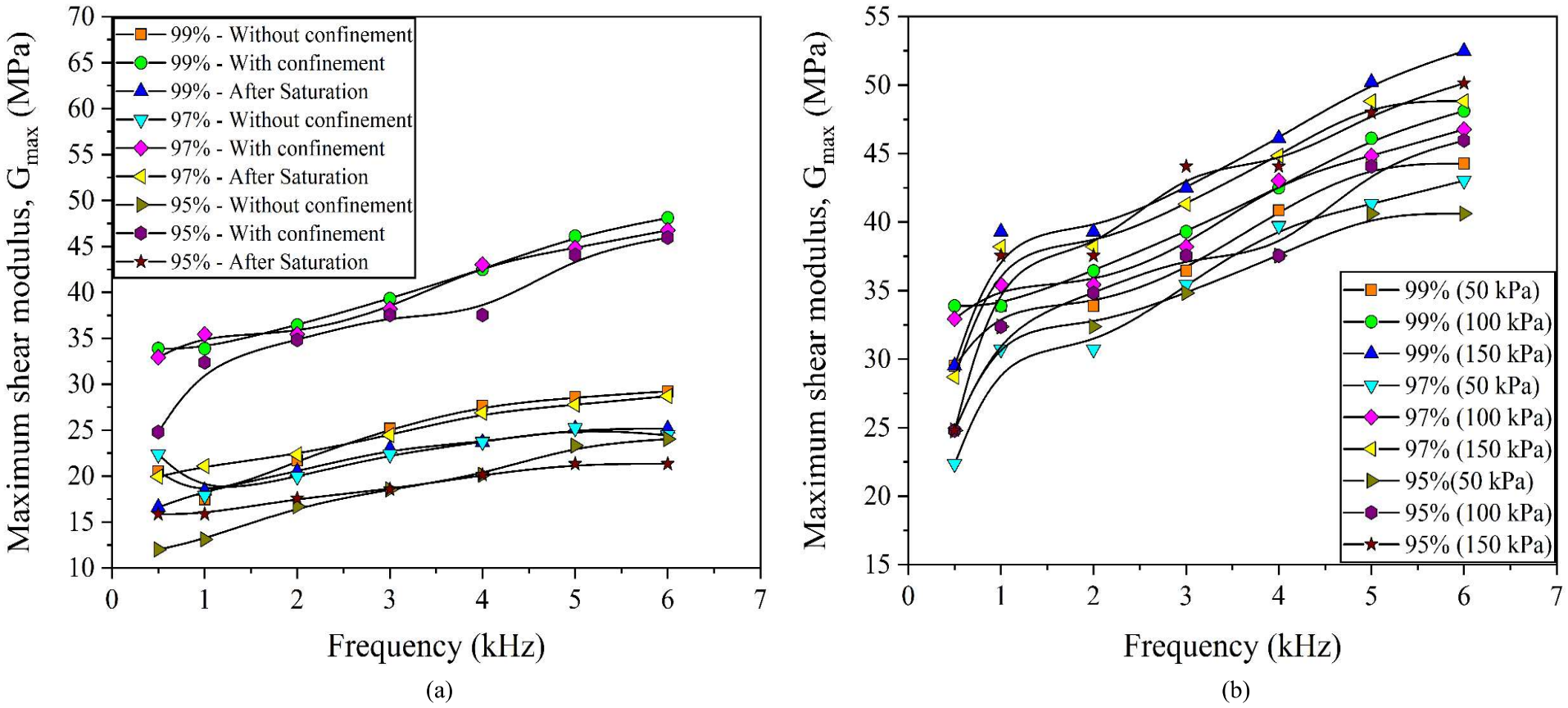

Fig. 9.7. Maximum shear modulus illustration of local soil considering (a) all conditions and (b) under confinement without saturation.

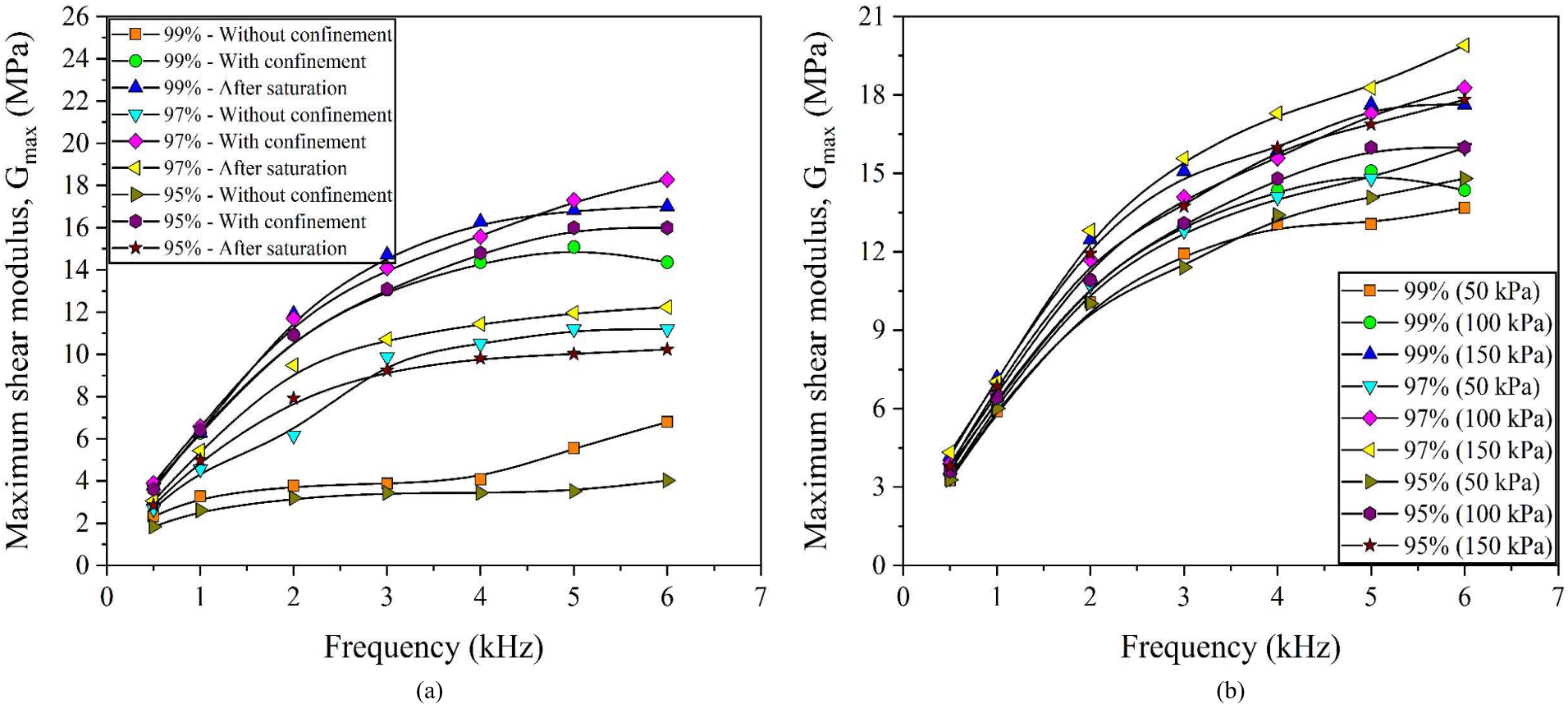

Fig. 9.8. Maximum shear modulus illustration of stratified soil-ash deposit considering (a) all conditions and (b) under confinement without saturation.

9.3.3 Assessment of Normalized Shear Modulus and Model Fitting

The normalized shear modulus (G/G_{max}) was calculated in order to make it dimensionless, so that its comparison and implementation could be convenient. The maximum shear modulus has been evaluated for the same condition as performed in the high strain cyclic triaxial test. Therefore, the particular specific condition can be implemented for the estimation of G/G_{max}. The normalized shear modulus for all the soil combination has been shown in Fig. 9.9. The data points of plot between G/G_{max} vs γ (shear strain) has been fitted with multiple models given by various researchers (Hardin 1978; Vucetic and Dobry 1991; Chattaraj and Sengupta 2017). After performing numerous iterations, the hyperbolic function was predicted better results than that of the other available models. The expression of the hyperbolic function is presented below:

$$\frac{G}{G_{max}} = \frac{1}{1+\left(\frac{\gamma}{a}\right)^{b}} \tag{9.1}$$

Where, G/G_{max} is the normalized shear modulus, γ is the cyclic shear strain (%), a & b are fitting parameters.

The hyperbolic fitting of the fly ash, local soil, and stratified soil-ash deposit are presented in Fig. 9.10. From the plot, this can be observed that the coefficient of determination (R^2) is found to be 0.76, 0.87, & 0.74 in the case of fly ash, local soil, and stratified soil-ash deposit respectively. These values can be further improved by conducting more experiments or with higher number of data points. This model will helpful in the interpolation or extrapolation of G/G_{max} at a lower or higher range of shearing strain.

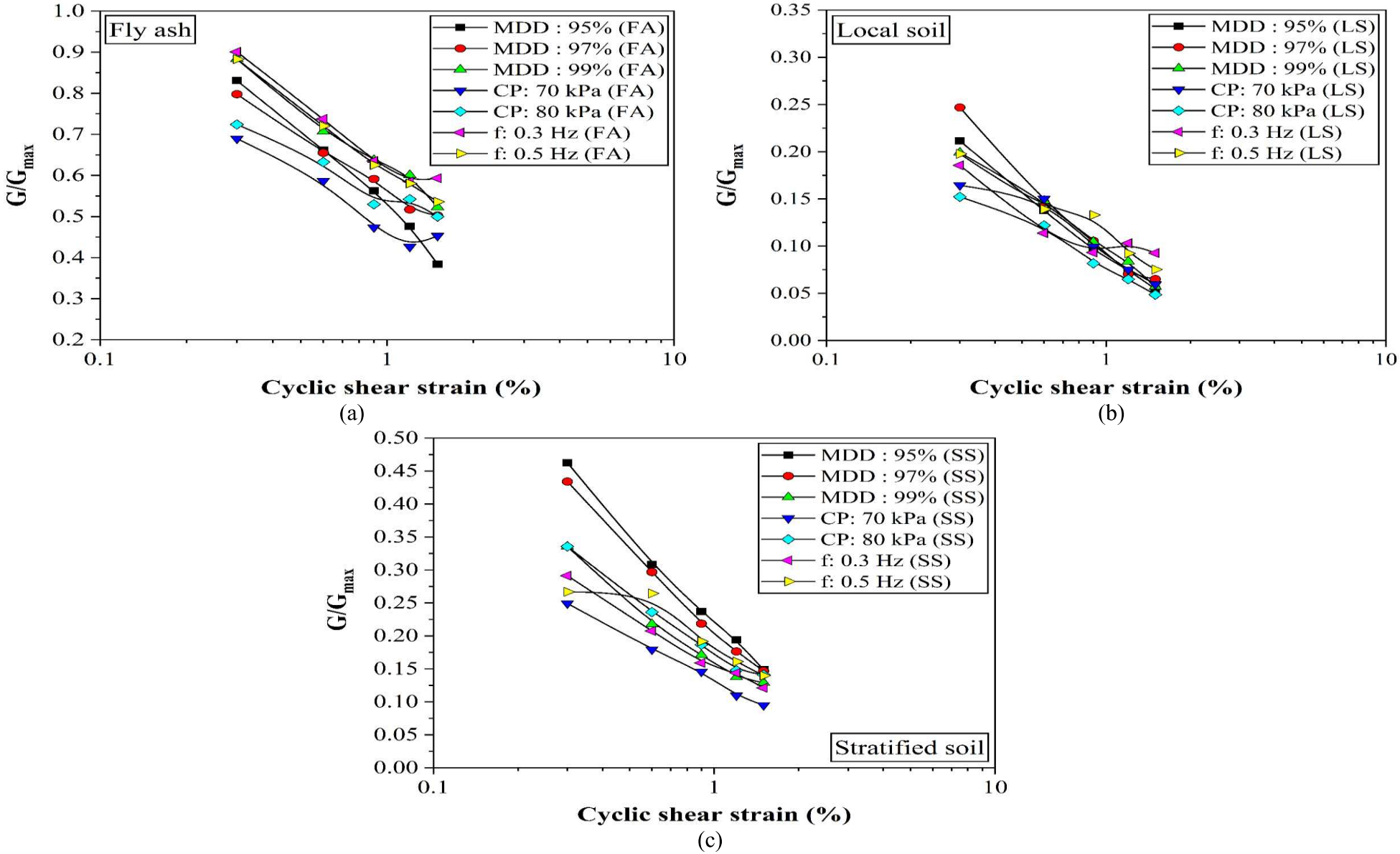

Fig. 9.9. Normalized shear modulus plot of homogeneous and stratified soil-ash deposit.

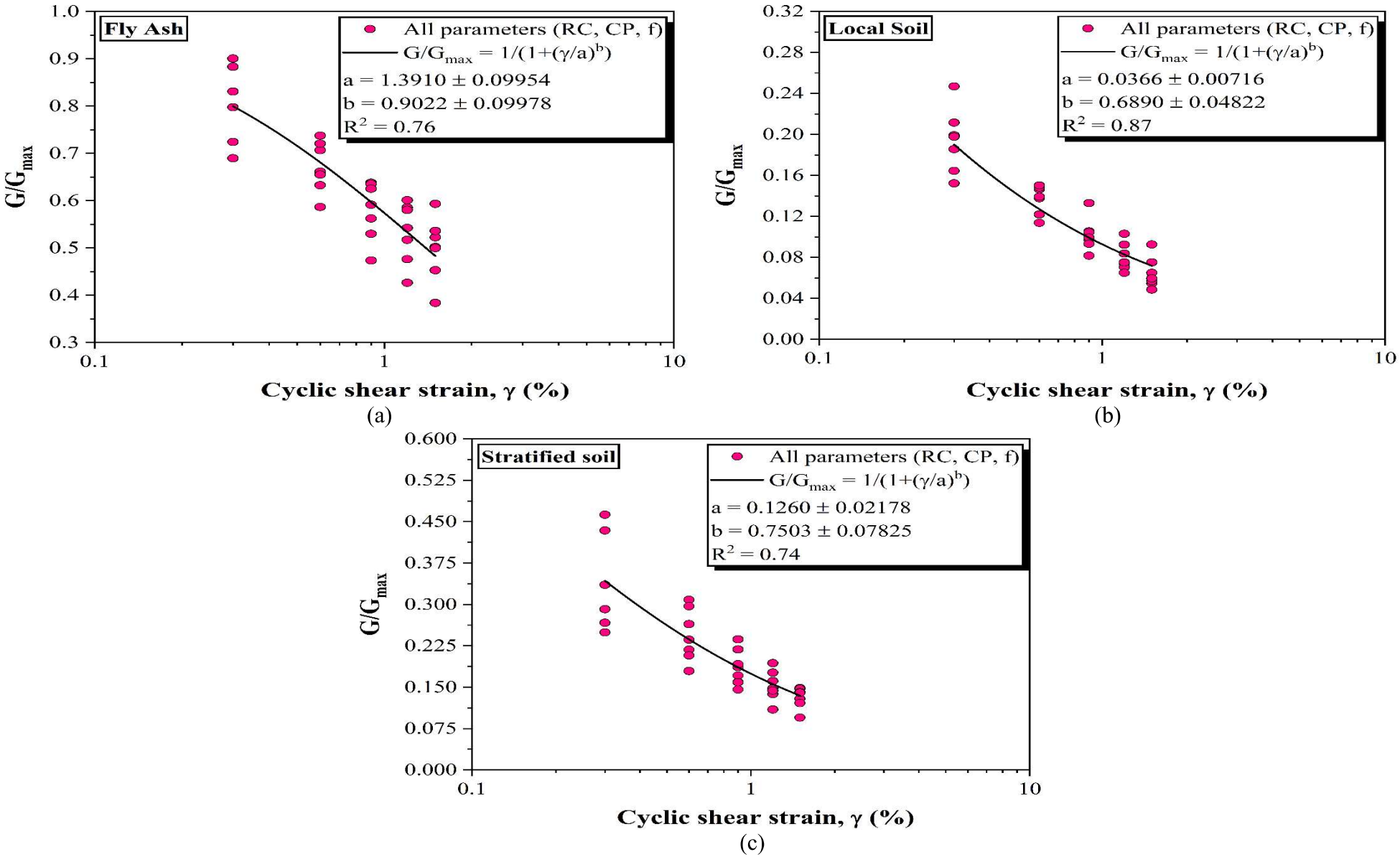

Fig. 9.10. Hyperbolic model fitting for modulus reduction curve of (a) fly ash, (b) local soil, and (c) stratified soil-ash deposit.

9.3.4 Assessment of Damping Ratio and Model Fitting

In the present study, damping ratio has been determined using three approaches, (a) symmetric hysteresis loop (SHL), (b) asymmetric hysteresis loop (ASHL), and (c) modified ASTM. As discussed in the previous chapter, the ASHL approach has observed many advantages due to the involvement of asymmetricity in its damping calculations. Hence, damping ratio was determined using ASHL approach that has been reported in Fig. 9.11. These results show a clear incremental trend of damping with shear strain with peak at 1% shear strain and then decreases, as observed by Kumar et al. (2017). There are various damping ratio models were given by several researchers considering void ratio, shear strain, effective confining pressure, and atmospheric pressure as input parameters (Hardin and Drnevich 1972; Borden et al. 1996; Chattaraj and Sengupta 2017; Amir-Faryar et al. 2017). Among these, Amir-Faryar et al. (2017) attempted to establish a universal model for the normalized shear modulus and damping ratio that could be applied for the homogeneous soil as well as fibre reinforced soil. After multiple trial, the hyperbolic damping model was found best fitted for the present study data rather than the universal model. Hence, this model has been implemented for the prediction of damping ratio at lower and higher shear strain. The hyperbolic model used for the prediction of damping ratio has been expressed below in Eq. 9.2.

$$D = \frac{(c \times \gamma)}{(1 + d \times \gamma)} \tag{9.2}$$

Where, D is the damping ratio, γ is the cyclic shear strain (%), c & d are model coefficient.

The hyperbolic damping model fitting of the fly ash, local soil, and stratified soil-ash deposits are presented in Fig. 9.12. From the plot, this can be inferred that the coefficient of determination (R^2) is found to be 0.88, 0.78, & 0.96 in the case of fly ash, local soil, and stratified soil-ash deposits respectively.

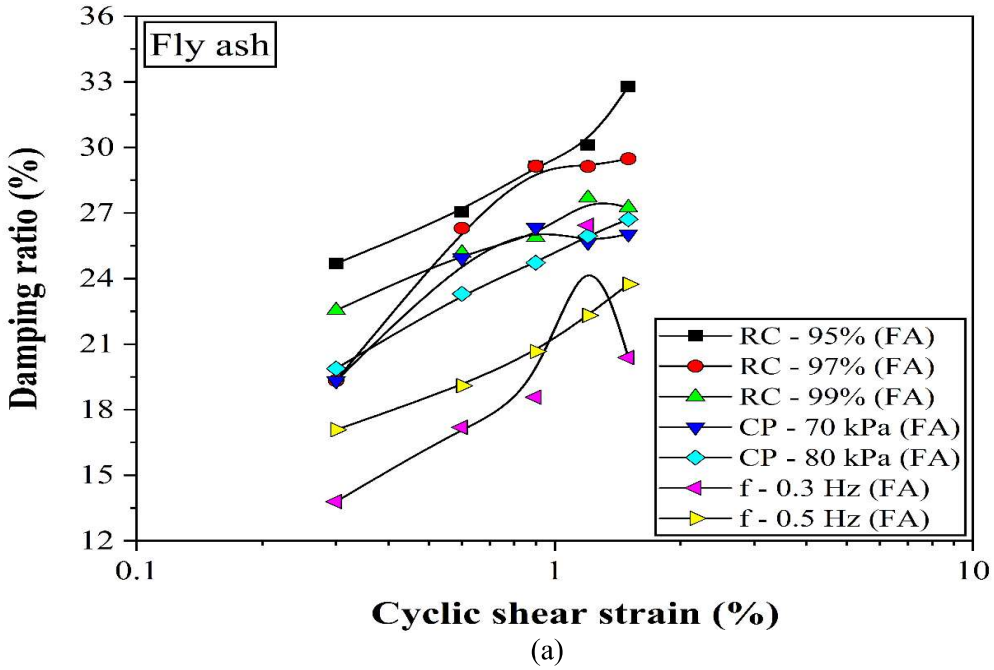
Fly ash
Damping ratio (%)
Cyclic shear strain (%)
RC - 95% (FA)
RC - 97% (FA)
RC - 99% (FA)
CP - 70 kPa (FA)
CP - 80 kPa (FA)
f - 0.3 Hz (FA)
f - 0.5 Hz (FA)

(a)

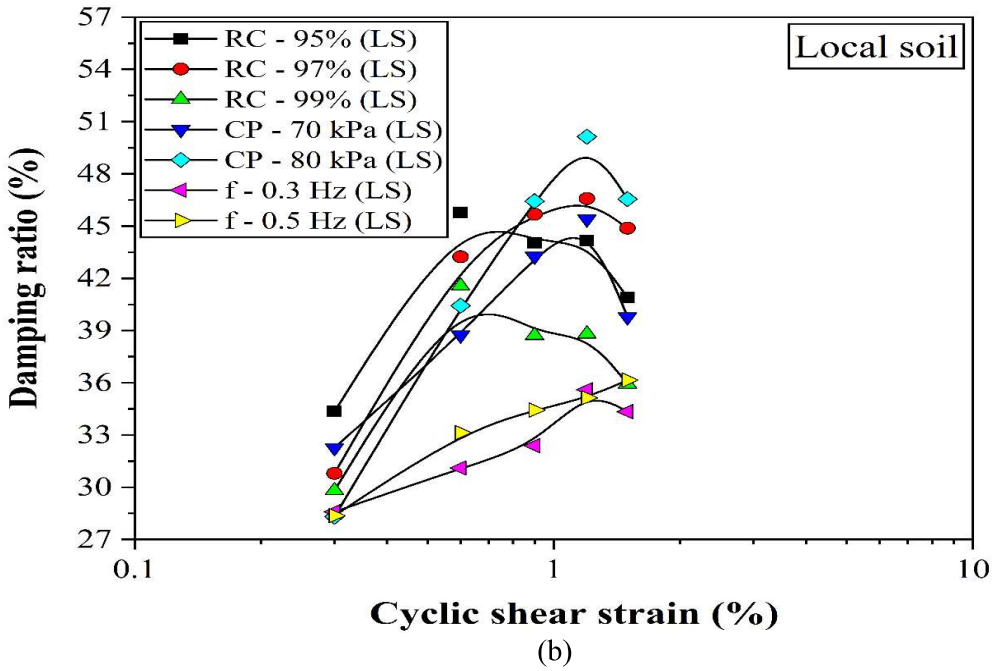
Local soil
Damping ratio (%)
Cyclic shear strain (%)
RC - 95% (LS)
RC - 97% (LS)
RC - 99% (LS)
CP - 70 kPa (LS)
CP - 80 kPa (LS)
f - 0.3 Hz (LS)
f - 0.5 Hz (LS)

(b)

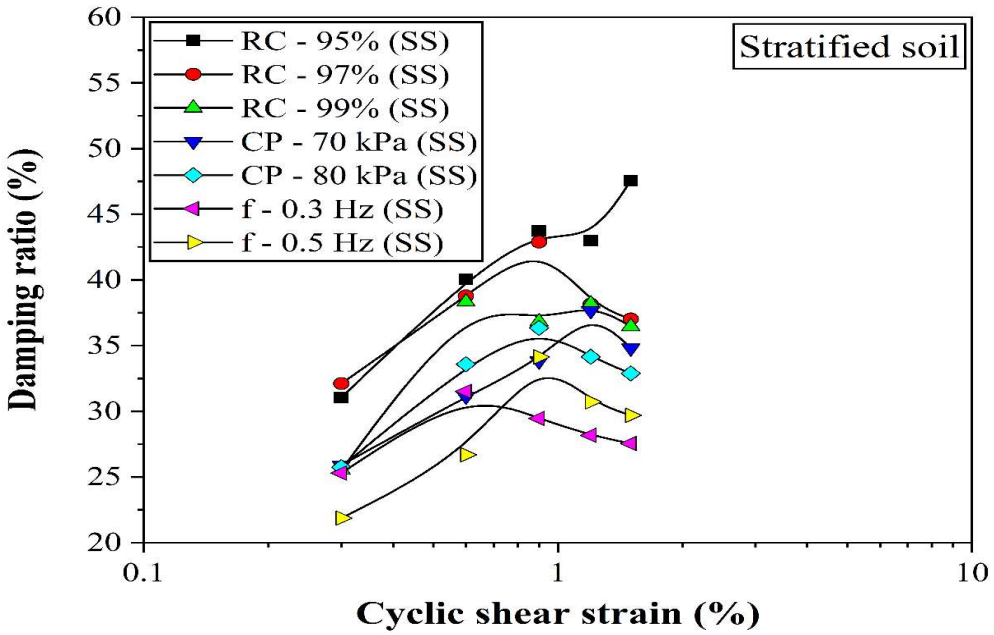

(c)

Fig. 9.11. Damping response of the homogeneous and stratified soil-ash deposits.

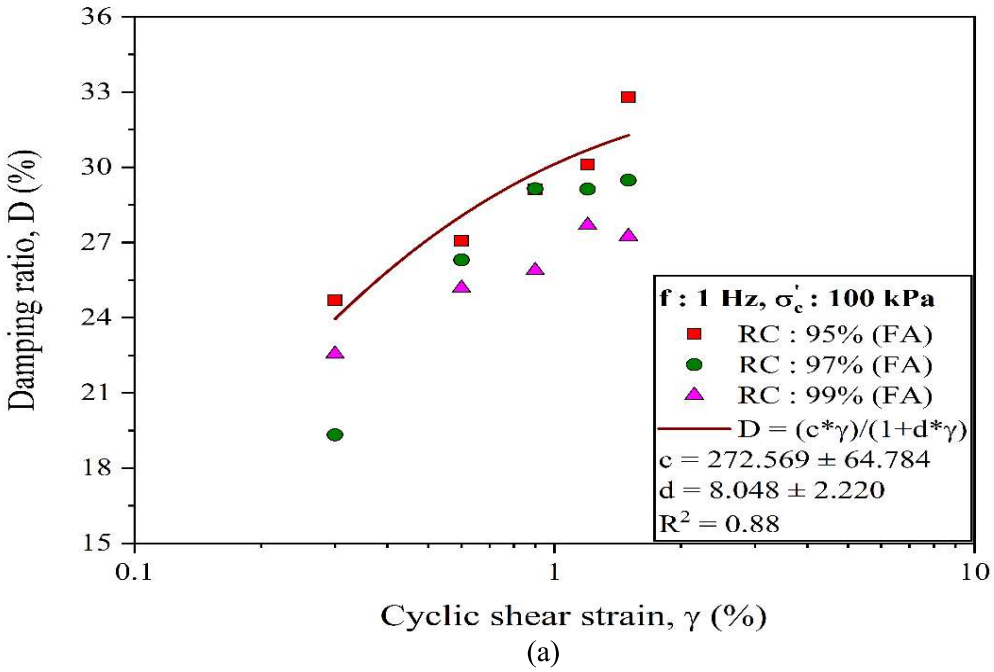

(a)

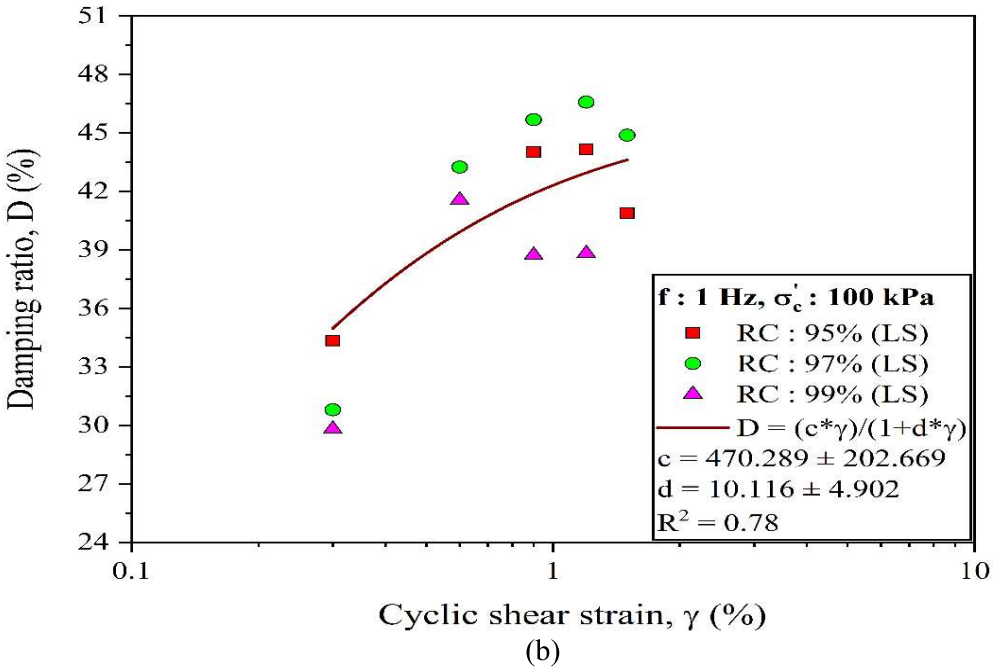

(b)

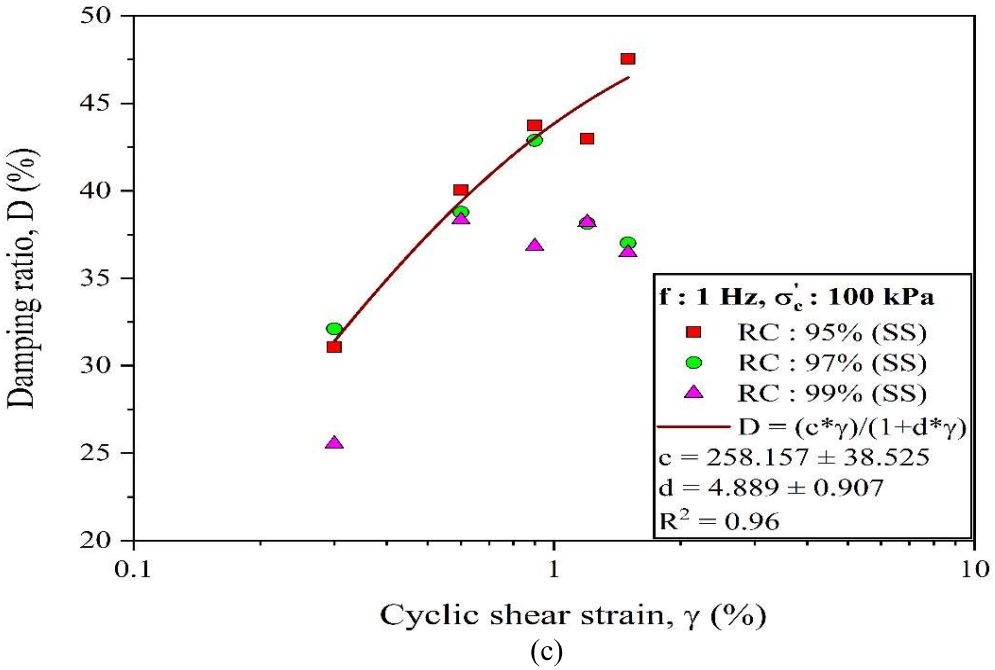

(c)

Fig. 9.12. Hyperbolic model fitting of damping response of fly ash, local soil, and stratified soil-ash deposits.

9.3.5 Development of Excess Pore Pressure Ratio Response Model using Strain Energy Approach

The pore pressure response has been experimentally measured with the help of pore pressure sensor installed at the bottom of the triaxial cell system. The pore pressure records of all the samples were established after taking into account all the relevant factors, including relative compaction, loading frequency, and effective confining pressure at high shearing strain. These responses have been utilized to calculate the excess pore pressure ratio, whereas the strain energy has been calculated using the hysteresis loop. The excess pore pressure ratio (r_u) is defined as the ratio of the excess pore pressure and the initial mean confining pressure. However, the strain energy ratio (W/W_{Liq}) is the ratio between strain energy per unit volume for a specific cycle and the cumulative strain energy per unit volume required for the sample till liquefaction. The combined response of the excess pore pressure ratio versus strain energy ratio considering all the independent variables for fly ash, local soil, and stratified soil-ash deposit are presented in Fig. 9.13, 9.14, 9.15 respectively. The r_u versus w/w_{Liq} plot is significantly dependent on all the parameters considered. The development of pore pressure is increased with the increase in frequency, relative compaction, and effective confining pressure; on contrast it decreases with the increase in shear strain. The rise in r_u is rapid during the initial cycles till 0.4 to 0.6 (r_u) and then increases linearly with the increase in W/W_{Liq}. On the other hand, local soil and stratified soil-ash deposit shows a similar response of r_u versus W/W_{Liq} i.e., achieved approximately 70 to 90% of the pore pressure generation during the initial phase of the loading. The plot of r_u versus w/w_{Liq} has been fitted to the excess pore pressure model as discussed by Jafarian et al. (2012). The expression of the excess pore pressure model is discussed below:

$$r_u = \left(\frac{\propto^{\frac{w}{w_{liq}}} - 1}{\propto - 1} \right)^{\beta} \quad (9.3)$$

where, r_u: excess pore pressure ratio, α and β is the calibration parameters, W/W_{Liq}: strain energy ratio.

Since, the r_u versus w/w_{Liq} plot consists of a large set of data with multiple fluctuations, therefore an attempt has been made to fit these data with upper and lower smooth profile. Hence, from the Fig. Fig. 9.13-9.15, the upper and lower limit profile of r_u versus w/w_{Liq} plot has been taken in order to cover the complete range of the data presented. These upper and lower limit profiles were incorporated for the determination of calibration factors α & β. The plot of r_u versus w/w_{Liq} fitted in the above model has been presented in Fig. Fig. 9.16 (a), 9.16 (b), and 9.16 (c) for the fly ash, local soil, and stratified soil-ash deposit respectively. The range of α lies between 0.05-1.9, 0.069-1.8, 0.04-1.48 for the fly ash, local soil and stratified soil-ash deposit respectively. Similarly, the range of β lies between 0.31-2.85, 0.15-0.54, 0.98-0.15 in the case of fly ash, local soil and stratified soil-ash deposit respectively. The ratio of strain energy per unit volume is the only parameter required for the estimation of r_u in the model, and this is the more realistic parameter that can be directly correlated to the field. The development of the excess pore pressure is a useful tool for the prediction of liquefaction failure. Hence, this simplified model can be used for the determination of the excess pore pressure ratio for similar kind of soil under different controlled environmental conditions.

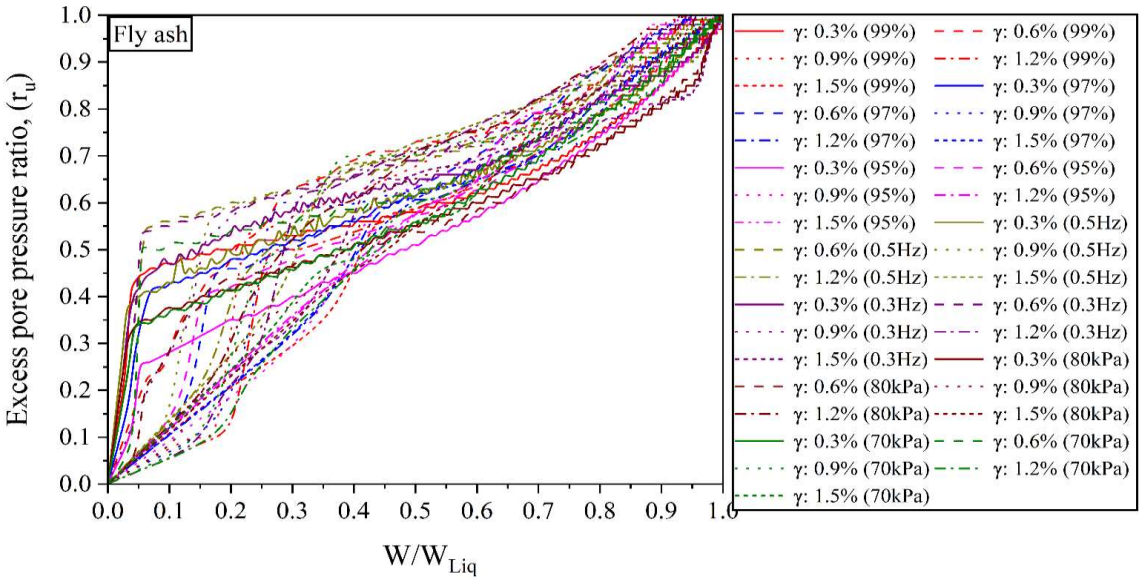

Fig. 9.13. The graphical illustration between excess pore pressure ratio and strain energy ratio for a particular density, frequency, and confining pressure for fly ash.

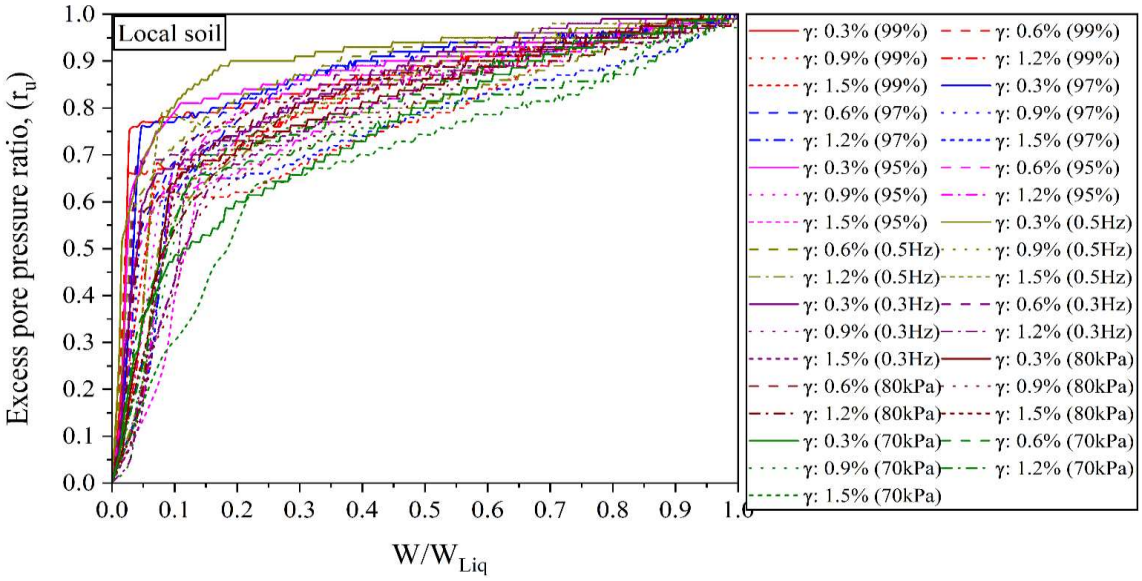

Fig. 9.14. The graphical illustration between excess pore pressure ratio and strain energy ratio for a particular density, frequency, and confining pressure for local soil.

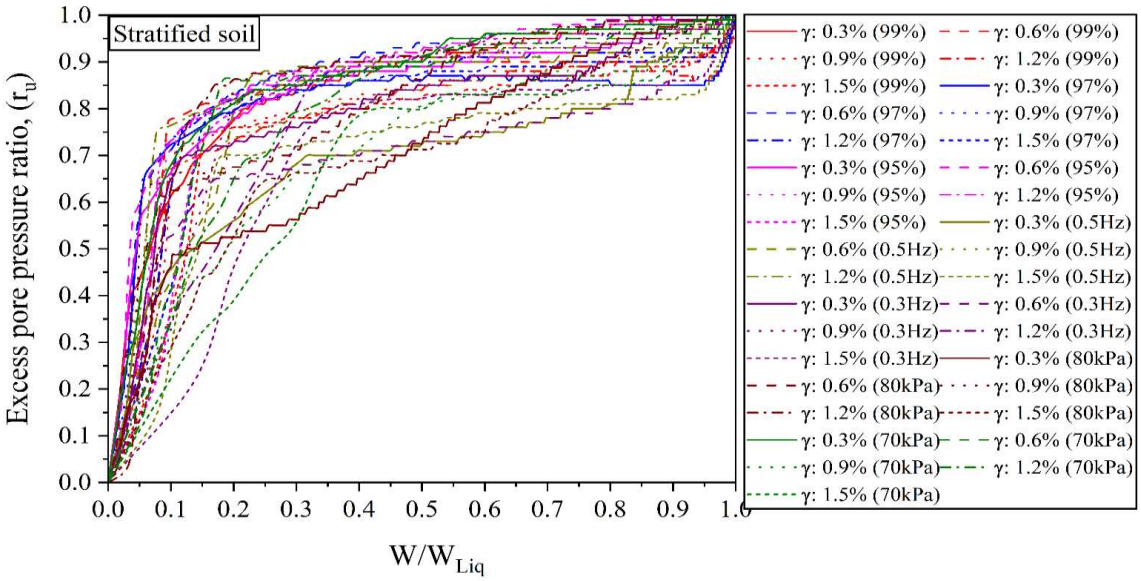

Fig. 9.15. The graphical illustration between excess pore pressure ratio and strain energy ratio for a particular density, frequency, and confining pressure for the stratified soil-ash deposit.

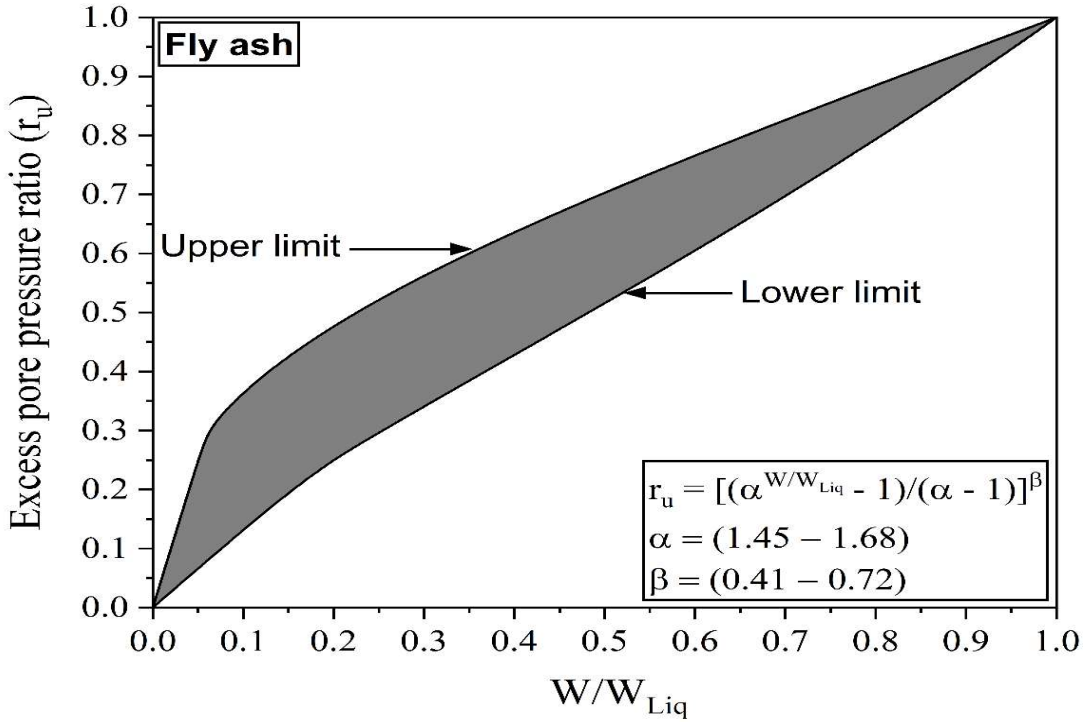

(a)

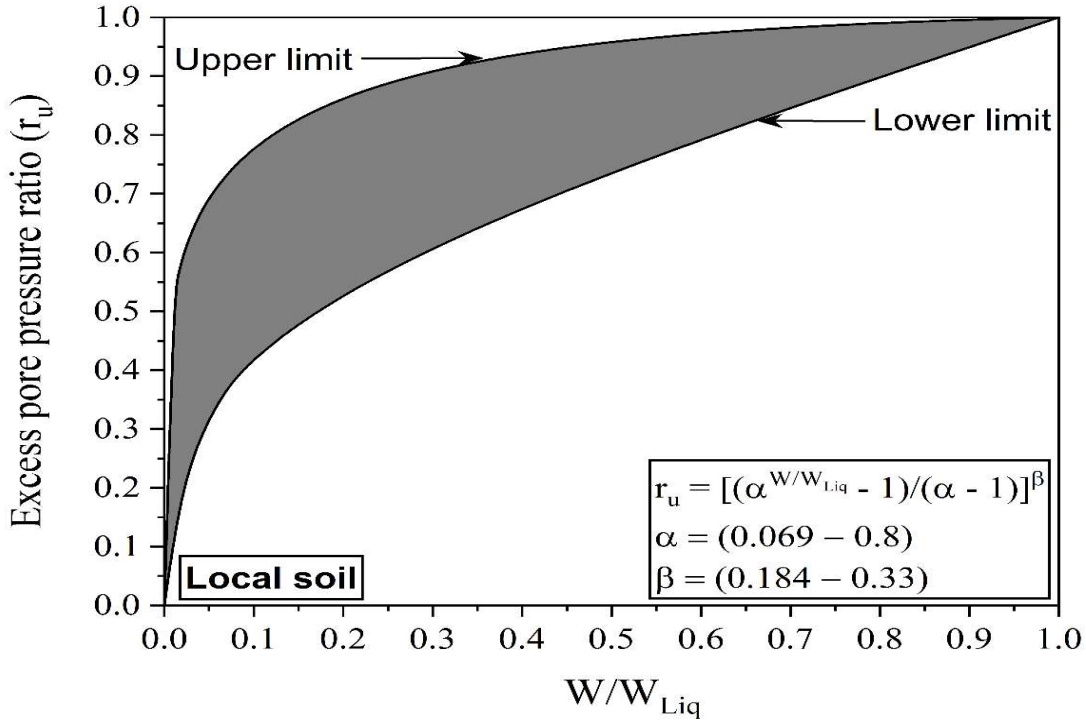

(b)

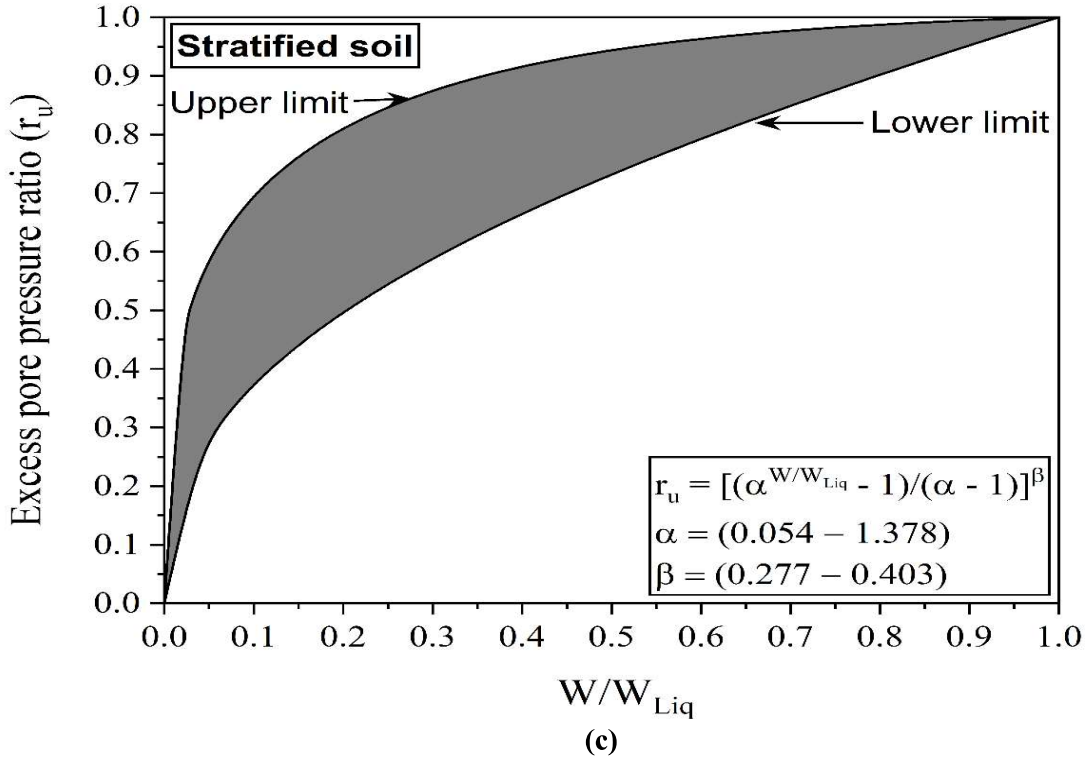

(c)

Fig. 9.16. Range of coefficients of pore pressure model obtained from the cyclic triaxial test conducted on the, (a) fly ash, (b) local soil, and (c) stratified soil-ash deposit.

9.4 SUMMARY

This chapter discussed about the evaluation of small-strain shear modulus or maximum shear modulus (G_{max}), and its normalization with high-strain dynamic shear modulus. Also, the models were fitted to the present generated normalized data and the excess pore pressure ratio of the homogeneous and stratified soil-ash deposits. The following conclusions can be drawn from the above-mentioned experimental analysis.

The outcomes of the study provide valuable insight into the estimation of shear wave travel time, the relationship between the maximum shear modulus (G_{max}) and confining pressure/frequency, the rate of G_{max} increase with frequency, and the application of hyperbolic models for G/G_{max} and damping ratio (D) estimation. The peak-to-peak method proved to be effective for estimating the wave travel time from the transmitter to the receiver. The study establishes a direct relationship between G_{max}, confining pressure, and the input wave frequency, with G_{max} increasing proportionally to these factors. The rate of G_{max} increase is initially high until 3-4 kHz of the input wave frequency but then decreases with further increase in frequency. The hyperbolic models demonstrate the best fit for G/G_{max} and damping ratio (D) estimation, making them suitable for predicting the stiffness properties of the homogeneous and stratified soil-ash deposits at low and high shear strains. Furthermore, an excess pore pressure ratio model has been developed, incorporating the energy ratio until liquefaction failure, with upper and lower boundary limits. This model enables the prediction of liquefaction failure in homogeneous and stratified soil-ash deposits based on the strain energy stored. Overall, these findings contribute to the understanding and prediction of the shear wave travel time, shear modulus behavior, stiffness properties, and liquefaction failure in homogeneous and stratified soil-ash deposits. These insights can aid in

designing and assessing the performance of such deposits in various engineering applications.